Advances and Applications in Fluid Mechanics
Volume 3, Issue 2, 2008, Pages 175-196
Published online: May 8, 2008
This paper is available online at http://www.pphmj.com

THE INFLUENCE OF THERMAL MODULATION ON THE BREAKUP OF A LIQUID SHEET: LINEAR STABILITY ANALYSIS

H. LIU[1*], W. C. SCHREIBER[1] and L. HADJI[2]

[1]Department of Mechanical Engineering
The University of Alabama
Tuscaloosa Alabama 35487, U. S. A.

[2]Department of Mathematics
The University of Alabama
Tuscaloosa Alabama 35487, U. S. A.

Abstract

The linear stability of a planar inviscid liquid sheet moving through a surrounding gas is examined. The analysis investigates the effect of an externally imposed time modulation of the gas temperature. These thermal perturbations in the gas layer are assumed to influence the air-gas interfacial tension coefficient. It is shown that the interface stability characteristics are described by a Mathieu equation, the coefficients of which are functions of the Weber number, the time modulation frequency, the gas/liquid density ratio, and the amplitude of the imposed temperature modulation. The maximum growth rate is determined as function of these physical parameters and the effect of the time modulation isolated.

Introduction

The phenomenon of liquid sheet or jet breakup is omnipresent in a

Keywords and phrases: hydrodynamic stability, liquid sheet, atomization, thermal modulation, surface tension.
*Corresponding author
Communicated by K. K. Azad
Received November 29, 2007

wide variety of industrial processes. A primary need for studies of liquid sheet breakup stems from the need for understanding the conditions necessary for effective fuel atomization in several types of spray combustion applications. See, for example, works by Clanet and Villermaux [1], Kim and Sirignano [4], Marmottant and Villermaux [7], Mansour and Chigier [6], Park et al. [8], and Sirignano and Mehring [9]. The classical works of Squire [10] and Hagerty and Shea [3] considered the temporal linear stability analysis for an inviscid liquid sheet of uniform thickness in a surrounding gas medium. They investigated the linear response to both symmetrical and antisymmetrical disturbance and found that the latter is the dominant mode of instability that will eventually lead to the break up of the sheet and subsequent formation of droplets. The main mechanism of instability was isolated to consist of the forces that take place at the interface between the liquid and the gas medium, namely aerodynamic advective and capillary forces. The disturbance growth or decay is determined from a competition between the stabilizing capillary forces and the destabilizing aerodynamic force. This competition is described by the dimensionless Weber number defined by $We = \rho_L u_0^2 a/\sigma_0$, where ρ_L, u_0, a and σ_0 are, respectively, the liquid sheet density, velocity relative to the gas, thickness, and interface surface tension. The uniformly planar sheet becomes unstable whenever the Weber number exceeds some critical value.

Dombrowski and Hooper [2] derived a dispersion relation for the growth rate for long waves with infinitestimal amplitude, including the effects of surface tension, aerodynamic force, liquid viscosity, and the non-uniform stretching caused by gravity. They identified the wavelength at the largest growth rate. Li and Tankin [5] extended Dombrowski and Hooper's studies to derive a more general dispersion relation that encompasses both short and long waves. They isolated two distinct modes of instability for viscous liquid sheets, an aerodynamic mode and a viscous mode. It was also found that symmetrical disturbances control the instability process for very small Weber number; while antisymmetrical disturbances dominate for large Weber number.

In this paper, we consider the effect of thermal modulations of the surrounding gas medium on the instability. The time-periodic variation of

the temperature in the surrounding gas medium, which is externally imposed, is assumed to influence only the interfacial properties of the liquid sheet. The liquid's bulk properties are unaltered; thus, only the liquid's coefficient of the surface tension is affected by the temperature changes in the adjacent surrounding gas. The fluctuation of the air temperature is assumed to be time periodic with an angular frequency ω and amplitude δ, i.e., $T_{air} = T_0 + \delta\cos(\omega t)$. The effect of the frequency ω on the liquid sheet instability is investigated for the case of an inviscid fluid.

Governing Equations

For the inviscid liquid sheet, assume u and w are the x and y liquid velocity components, and p is the pressure variation resulting from a disturbance. These quantities are presumed to be very small. The equation of continuity and motion is linearized by neglecting all nonlinear terms in these small disturbance quantities, and can be expressed as follows:

$$\frac{\partial u}{\partial t} = -\frac{1}{\rho_L}\frac{\partial p}{\partial x}, \tag{1}$$

$$\frac{\partial w}{\partial t} = -\frac{1}{\rho_L}\frac{\partial p}{\partial z}, \tag{2}$$

$$\frac{\partial u}{\partial x} + \frac{\partial w}{\partial z} = 0. \tag{3}$$

The effect of the surrounding gas medium on the instability of the liquid sheet comes about through the normal stress in the boundary condition. The gas medium is assumed to be inviscid, and stationary before the disturbance commences. The governing equations, in a frame of reference moving with a velocity u_0, for the disturbed gas motion are:

$$\frac{\partial u'}{\partial t} = -\frac{1}{\rho'}\frac{\partial p'}{\partial x} - \frac{\partial u'}{\partial x}u_0, \tag{4}$$

$$\frac{\partial w'}{\partial t} = -\frac{1}{\rho'}\frac{\partial p'}{\partial z} - \frac{\partial w'}{\partial x}u_0, \tag{5}$$

$$\frac{\partial u'}{\partial x} + \frac{\partial z'}{\partial w} = 0. \tag{6}$$

The boundary conditions are

$$w = \frac{\partial h}{\partial t} \quad \text{at } z = h = a + \eta, \tag{7}$$

$$w = 0 \quad \text{at } z = 0, \tag{8}$$

$$u' \to 0 \quad w' \to 0 \quad p' \to 0 \quad \text{at } z = \infty, \tag{9}$$

$$w' = \frac{\partial h}{\partial t} + \frac{\partial h}{\partial x} u_0 \quad \text{at } z = h = a + \eta, \tag{10}$$

$$-p + p' = \sigma \frac{\partial^2 h}{\partial x^2} \quad \text{at } z = h = a + \eta. \tag{11}$$

Let $\sigma = \sigma_0 + \sigma_T(T - T_0)$ and $T - T_0 = \delta \cos(\omega t)$. Then $-p + p' = \sigma \dfrac{\partial^2 h}{\partial x^2}$ becomes

$$-p + p' = (\sigma_0 + \sigma_T \delta \cos(\omega t)) \frac{\partial^2 h}{\partial x^2}. \tag{12}$$

Letting $\varepsilon = \dfrac{\delta \sigma_T}{\sigma_0}$, we get

$$-p + p' = \sigma_0 (1 + \varepsilon) \frac{\partial^2 h}{\partial x^2}. \tag{13}$$

Upon introducing the potential functions ϕ and ϕ' as

$$u = \phi_x, \quad w = \phi_z, \tag{14}$$

$$u' = \phi'_x, \quad w' = \phi'_z, \tag{15}$$

we obtain

$$\nabla^2 \phi = 0, \tag{16}$$

$$\nabla^2 \phi' = 0. \tag{17}$$

The Fourier transform of equation (16) yields

$$D^2 \hat{\phi} - k^2 \hat{\phi} = 0 \tag{18}$$

the solution of which satisfies the boundary conditions given in (8) and is

$$\hat{\phi} = A \cosh(kz). \tag{19}$$

Applying boundary condition (7), we find

$$D\hat{\phi}(a) = \frac{\partial\hat{\eta}}{\partial t} = Ak\sinh(ak), \tag{20}$$

where

$$A = \frac{\hat{\eta}_t}{k\sinh(ak)}. \tag{21}$$

The solutions of equations (1) and (2), then give

$$\hat{p} = \frac{-\rho_L\hat{\eta}_{tt}}{k\sinh(ak)}\cosh(kz), \tag{22}$$

$$\hat{p}(a) = \frac{-\rho_L}{k}\coth(ak)\hat{\eta}_{tt}. \tag{23}$$

The Fourier transform of equation (17) is

$$D^2\hat{\phi}' - k^2\hat{\phi}' = 0. \tag{24}$$

The solution of which satisfies the boundary conditions given in (9) and is

$$\hat{\phi}' = Be^{-kz}. \tag{25}$$

According to boundary condition (5), then

$$D\hat{\phi}'(a) = -kBe^{-ka} = \frac{\partial\hat{\eta}}{\partial t} - iku_0\hat{\eta}. \tag{26}$$

We get

$$B = \frac{-e^{ka}}{k}(\hat{\eta}_t - iku_0\hat{\eta}), \tag{27}$$

$$\hat{p}' = \frac{\rho'}{k}(\hat{\eta}_{tt} - iku_0\hat{\eta}_t)e^{-k(z-a)} - i\rho'(\hat{\eta}_t - iku_0\hat{\eta})e^{-k(z-a)}, \tag{28}$$

$$\hat{p}'(a) = \frac{\rho'}{k}\hat{\eta}_{tt} - 2i\rho' u_0\hat{\eta}_t - k\rho'\hat{\eta}. \tag{29}$$

Put (23) and (29) into boundary condition (11) and Fourier transform the right hand part of equation (11), we get

$$\frac{1}{k}\coth(ka)\hat{\eta}_{tt} + \frac{Q}{k}\hat{\eta}_{tt} - 2iQu_0\hat{\eta}_t - kQ\hat{\eta} = -k^2\sigma_0(1+\varepsilon\cos(\omega t))\hat{\eta}_t, \tag{30}$$

where $R = \sigma_0/\rho_L u_0^2 a$ is the inverse Weber number, and $Q = \rho'/\rho_L$ is the density ratio. Upon rearranging the above equations, we have

$$\hat{\eta}_{tt} + \frac{2iku_0 Q}{\coth(ak) + Q}\hat{\eta}_t + \frac{k^2(k\sigma_0 - Q + k\sigma_0 \varepsilon \cos(\omega t))}{\coth(ak) + Q}\hat{\eta} = 0. \tag{31}$$

The form of the solution for the above equation is

$$\hat{\eta} = e^{-\frac{iku_0 Q}{\coth(ak)+Q}t} f(t). \tag{32}$$

Put this solution into equation (31), we get following equation:

$$\frac{d^2 f}{dt^2} + u_0^2/a^2\left[\frac{K^3 R - K^2 Q}{\coth(K)+Q} + \frac{K^2 Q^2}{(\coth(K)+Q)^2} + \frac{K^3 R\varepsilon}{\coth(K)+Q}\cos(\omega t)\right] f = 0, \tag{33}$$

where $K = ka$ is the dimensionless wavenumber.

Setting $\omega t = 2\tau$, we get

$$\frac{d^2 f}{d\tau^2} + \frac{4u_0^2}{\omega^2 a^2}\left[\frac{K^3 R - K^2 Q}{\coth(K)+Q} + \frac{K^2 Q^2}{(\coth(K)+Q)^2} + \frac{K^3 R\varepsilon}{\coth(K)+Q}\cos(2\tau)\right] f = 0. \tag{34}$$

For an antisymmetrical disturbance, we can get the following equation using a similar derivation:

$$\frac{d^2 f}{d\tau^2} + \frac{4u_0^2}{\omega^2 a^2}\left[\frac{K^3 R - K^2 Q}{\tanh(K)+Q} + \frac{K^2 Q^2}{(\tanh(K)+Q)^2} + \frac{K^3 R\varepsilon}{\tanh(K)+Q}\cos(2\tau)\right] f = 0. \tag{35}$$

Introducing a nondimensional frequency $\hat{\omega} = \omega/(u_0/a)$, and (34) and (35) become

$$\frac{d^2 f}{d\tau^2} + \frac{4}{\hat{\omega}^2}\left[\frac{K^3 R - K^2 Q}{\coth(K)+Q} + \frac{K^2 Q^2}{(\coth(K)+Q)^2} + \frac{K^3 R\varepsilon}{\coth(K)+Q}\cos(2\tau)\right] f = 0, \tag{36}$$

$$\frac{d^2 f}{d\tau^2} + \frac{4}{\hat{\omega}^2}\left[\frac{K^3 R - K^2 Q}{\tanh(K)+Q} + \frac{K^2 Q^2}{(\tanh(K)+Q)^2} + \frac{K^3 R\varepsilon}{\tanh(K)+Q}\cos(2\tau)\right] f = 0. \tag{37}$$

The above equations are known as the Mathieu equations which admit solutions of the form:

$$f(\tau) = (e^{i\nu\tau} + e^{-i\nu\tau})P(\tau), \tag{38}$$

where $\nu = \nu_R + i\nu_i$, and $P(\tau)$ is a periodic function, and ν_i determines the stability of Mathieu equations. If $\nu_i = 0$, the equations remain stable; otherwise, it is unstable. The absolute value of ν_i represents the growth rate of disturbance wave. The larger the absolute value of ν_i, the larger is the growth rate of the disturbance wave.

For Mathieu equations, the following equation should be satisfied

$$\cos(\pi\nu) - f(\pi) = 0; \tag{39}$$

and, then, the value of ν_i can be obtained from the above equation. To facilitate the analysis and compare with published results, $\hat{\upsilon}_i$ is defined as a dimensionless growth rate of the disturbance wave as $\hat{\nu}_i = \nu_i/(\sigma_0/\rho_L a^3)^{1/2} = \nu_i/(R u_0/a)$. The term $|\hat{\nu}_i|$ represents the nondimensional growth rate, and we define the gas Weber number as $We_2 = \dfrac{\rho' u_0^2 a}{\sigma_0}$.

Analysis and Discussion

Thermal modulation absent

Without the effect of thermal modulation, i.e., $\varepsilon = 0$, the equations take a very simple form.

For the symmetrical disturbance, we have

$$\frac{d^2 f}{dt^2} + \frac{u_0^2}{a^2}\left[\frac{K^3 R - K^2 Q}{\coth(K) + Q} + \frac{K^2 Q^2}{(\coth(K) + Q)^2}\right] f = 0. \tag{40}$$

For antisymmetrical disturbance

$$\frac{d^2 f}{dt^2} + \frac{u_0^2}{a^2}\left[\frac{K^3 R - K^2 Q}{\tanh(K) + Q} + \frac{K^2 Q^2}{(\tanh(K) + Q)^2}\right] f = 0. \tag{41}$$

In order to get a stable solution for the symmetrical disturbance, the equation below should be satisfied.

$$(K^3 R - K^2 Q)(\coth(K) + Q) + K^2 Q^2 > 0. \tag{42}$$

Solving equation (42) for R, we get

$$R > \frac{1}{K}\frac{Q\coth(K)}{Q+\coth(K)} \tag{43}$$

or equivalently,

$$We_2 < K + \frac{KQ}{\coth(K)}. \tag{44}$$

In order to get a stable solution for the antisymmetrical disturbance, the equation below should be satisfied

$$(K^3R - K^2Q)(\tanh(K) + Q) + K^2Q^2 > 0 \tag{45}$$

from which, we obtain,

$$R > \frac{1}{K}\frac{Q\tanh(K)}{Q+\tanh(K)} \tag{46}$$

or equivalently,

$$We_2 < K + \frac{KQ}{\tanh(K)}. \tag{47}$$

For long-wave disturbances, $K \ll 1$, $\tanh(K) \approx K$ and $\coth(K) \approx 1/K$; therefore, for a symmetrical disturbance

$$We_2 < K. \tag{48}$$

On the other hand, for short wave $K \gg 1$, $\tanh(K) \approx 1$, and $\coth(K) \approx 1$, then both (44) and (47) reduce to

$$We_2 < K + KQ. \tag{49}$$

Generally, equations (42) and (46) have to be solved numerically. This has been done and stability curves are presented in Figure 1 for a density ratio of $Q = 0.1$. In Figure 1, the region above the solid curve is the instability region for symmetrical disturbance, and the region above the dash curve is the instability region for antisymmetrical disturbance. Both instability regions are due to the aerodynamic interaction at the interface.

It is clear from Figure 1 that for inviscid liquid sheets, the instability range for symmetrical disturbances is wider than that for antisymmetrical disturbances. Both critical Weber numbers approach the same asymptotic value of $K + KQ$, from above for antisymmetrical disturbances and from below for symmetrical disturbances. The same instability range for each type disturbance has been obtained by Hagerty and Shea [3] and Li and Tankin [5], and thus our results are consistent with previous works in the absence of modulation.

The growth rate is obtained by solving equations (40) and (41). Figures 2 and 3 show the nondimensional growth rate $|\hat{\nu}_i|$ for an antisymmetrical disturbance and a symmetrical disturbance, respectively, where the density ratio $Q = 0.1$ and gas Weber number $We_2 = 4$. These results also mirror those obtained by Li and Tankin [5].

Figure 4 illustrates the aerodynamic instability of inviscid liquid sheet at small Weber numbers (Figure 4(a)) and at large Weber numbers (Figure 4(b)). The solid lines correspond to a symmetrical disturbance, and the dashed curves to an antisymmetrical disturbance. Figure 4(a) indicates that at very small gas Weber numbers, symmetrical disturbances have a larger growth rate than antisymmetrical ones and dominate the instability process. As the gas Weber number increases, the maximum growth rate for both types of disturbances increase; however, that of antisymmetrical disturbance increases faster and, above a certain gas Weber number, antisymmetrical disturbances become predominant in full agreement with the results obtained by Li and Tankin [5].

Thermal modulation case

The inclusion of thermal modulation is described by the Mathieu equations (36) and (37). For a demonstration we set $\hat{\omega} = 1$, $\varepsilon = 0.5$ and $Q = 0.1$. The solution of the Mathieu equations yields the location of the instability regions, shown as a three-dimensional plot in Figure 5, as a function of K and We_2.

The maximum growth rate of disturbance for a given Weber number, with K varying, is located in either the first instability region, which is

caused by aerodynamic forces or in the second instability region which is the lowest mode caused by thermal modulation. Only the first two instability regions, therefore, need to be considered when studying the instability analysis.

For a small Weber number, it is found that the maximum nondimensional growth rate of the disturbance is located in the second unstable region which is caused by thermal modulation, as illustrated in Figure 6 for a Weber number of 1.0, where the maximum growth rate for the first unstable region is 0.54. The maximum growth rate for the second unstable region is 0.78. The dominant wave number in the first unstable region is approximately equal to the dominant wave number without thermal modulation, which can be found from the comparison between Figures 6 and 7. The dominant wave number in the second unstable region is much larger than the dominant wave number in the first region. The dominant wave number with thermal modulation is somewhat larger than that without thermal modulation and will result in the smaller wavelength for thermal modulation case. As the Weber number increases, the maximum growth rates in both regions increase. However, the increase of the maximum growth rates in first unstable region is much faster than that in second unstable region. When the Weber number exceeds a certain value (in this case $We_2 = 2$ with symmetrical disturbance), the maximum growth rate of the first unstable region will be larger than that in second unstable region, shown as Figures 8 and 9. In Figure 8 ($We_2 = 3$), the maximum growth rate for first unstable region is 1.85, whereas the maximum growth rate for second unstable region is 1.75. In Figure 9, we examine the growth rate without thermal modulation ($We_2 = 4$) and learn that the maximum growth rate for first unstable region is 2.45, whereas the maximum growth rate for second unstable region is 2.2. With increasing Weber number, the maximum growth rate difference between in the first and second unstable region keep going up, shown as Figure 5. When maximum growth rate shift from the first unstable region to second unstable region, the dominant wave number jumps from a high value to a low value shown as Figure 10. This means the wavelength of maximum growth rate jumps to a high value,

which approximately equal to the wavelength of maximum growth rate without thermal modulation at the same Weber number. Similar results are obtained in the instability analysis of antisymmetrical disturbance. The maximum growth rate shifts from the second unstable region to the first unstable region when $We_2 = 1.25$, shown as Figure 10.

From Figure 10, it is clear that the whole dominant wave number of the antisymmetrical disturbance is always larger than that of symmetrical disturbance. It is also found the maximum growth rate of the antisymmetrical disturbance is larger than that of symmetrical disturbance shown as Figure 11. The antisymmetrical disturbance dominates the instability of liquid sheet.

For the next case considered, $\hat{\omega}$ is set to 5, Q equal to 0.1 and thermal modulation amplitude is held at 0.5. From Figure 12, it is found that maximum growth rates of symmetrical and antisymmetrical disturbance almost keep the same value. It means that both symmetrical and antisymmetrical disturbances are important under high frequency thermal modulation effect. From Figure 13, it is clear that maximum growth rate jumps from second unstable region to first unstable region at a very high Weber number. It illustrates that the second unstable region caused by thermal modulation dominates the instability of liquid sheet in a wider region compared with smaller frequency case. Also the maximum growth rate of high frequency is much larger than that of low frequency at low Weber number and will reduce the breakup time of liquid sheet.

The thermal modulation amplitude also affects the instability analysis of a liquid sheet. From Figure 14, we can see that the second unstable region control the instability of liquid sheet in a very small range. In this case, the maximum growth rate shifts from the second unstable region to the first unstable region at $We_2 = 0.3$ for antisymmetrical disturbance and shifts from the second unstable region to the first unstable region at $We_2 = 0.5$ for the symmetrical disturbance. Also the maximum growth rate of lower thermal amplitude is much smaller than that of high thermal amplitude at low Weber number. It means it will delay the breakup time of liquid sheet.

Conclusion

The paper examines the temporal instability of a moving thin inviscid liquid sheet in a heat conducting surrounding gas medium the temperature of which is assumed time modulated. The thermal effect acts in such a way as to modify the coefficient of interfacial surface tension. The instability is described by a Mathieu equation, the coefficients of which are function of the Weber number in the gas medium, the density ratio, the modulation frequency, and the modulation amplitude.

From the above discussion, it is found that both thermal modulation and aerodynamic forces can affect the liquid sheet breakup process. The thermal modulation dominates the liquid sheet breakup when the Weber number is small, and plays only a small role as the Weber number increases. The frequency and amplitude of the thermal modulation also affect the liquid sheet breakup. High frequency will result in short wavelength and short breakup time in low Weber number. High thermal modulation amplitude will widen the unstable region controlled by thermal modulation.

The effects of finite amplitude disturbances require a weakly nonlinear analysis. This is described in a follow-up paper.

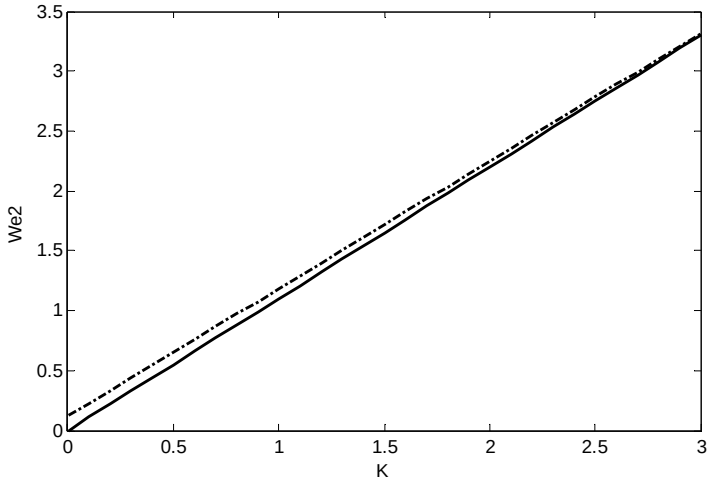

Figure 1. Critical Weber for inviscid liquid sheets ($Q = 0.1$) solid curve: symmetrical disturbance; dash curve: antisymmetrical disturbance.

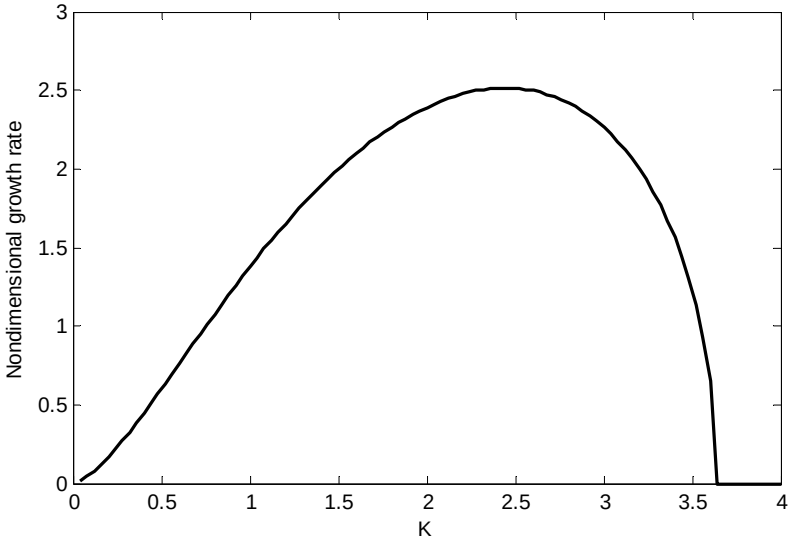

Figure 2. Nondimensional growth rate of a symmetrical disturbance, $Q = 0.1$ and $We_2 = 4$.

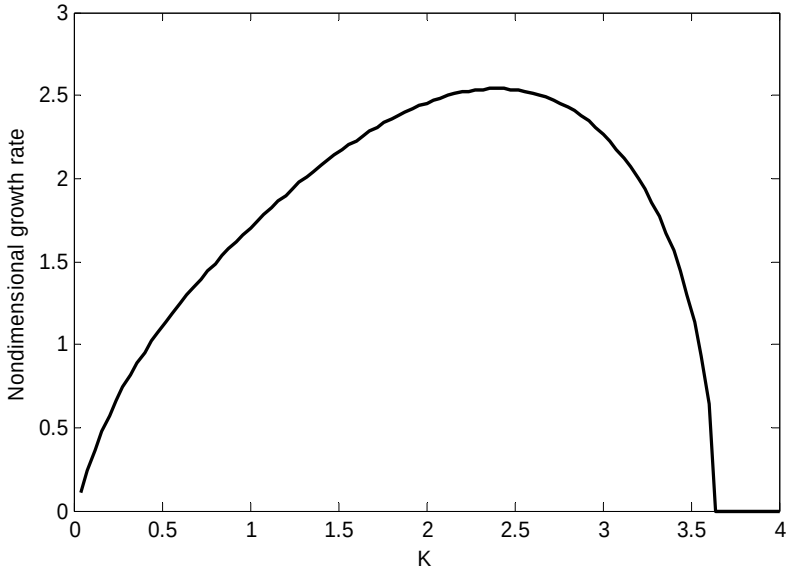

Figure 3. Nondimensional growth rate of an antisymmetrical disturbance, where $Q = 0.1$ and $We_2 = 4$.

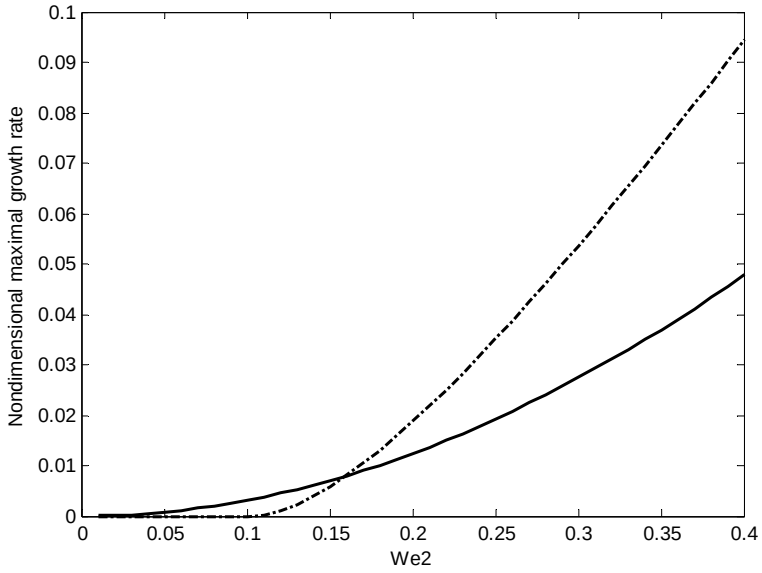

Figure 4(a)

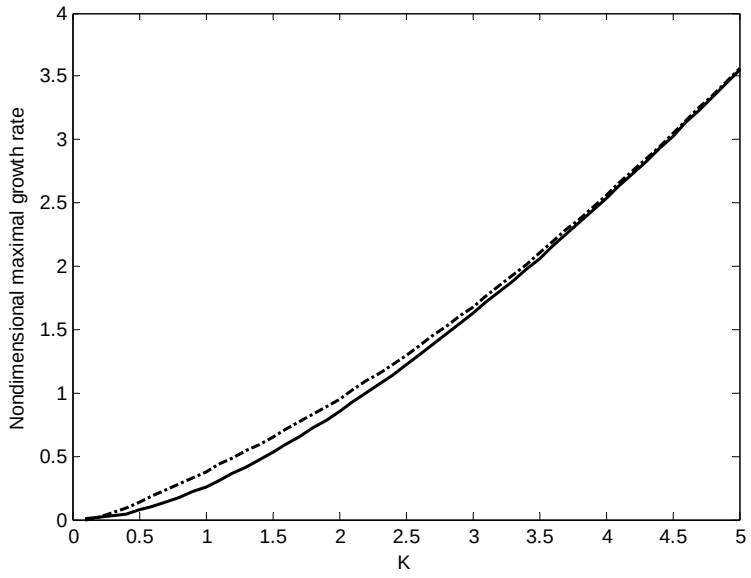

Figure 4(b)

Figure 4. Nondimensional growth rate of a disturbance at $Q = 0.1$ solid curve: symmetric disturbance, dash line: antisymmetrical disturbance.

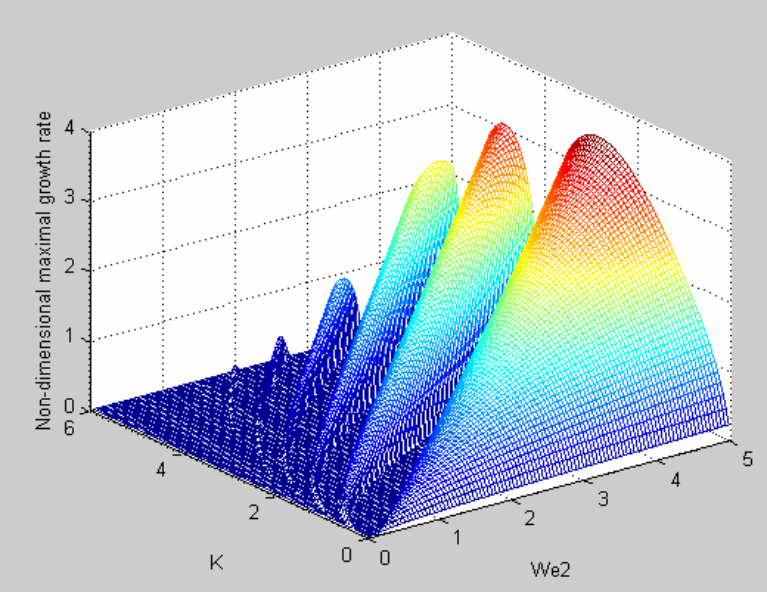

Figure 5. The unstable regions of liquid sheet with thermal modulation ($\hat{\omega} = 1$, $\varepsilon = 0.5$) at $Q = 0.1$.

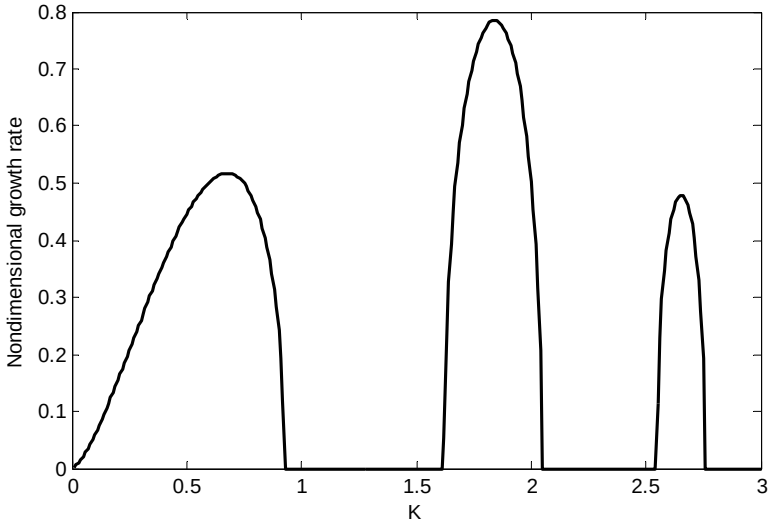

Figure 6. Nondimensional growth rate of an antisymmetrical disturbance with thermal modulation ($\hat{\omega} = 1$, $\varepsilon = 0.5$) at $Q = 0.1$ and $We_2 = 1$.

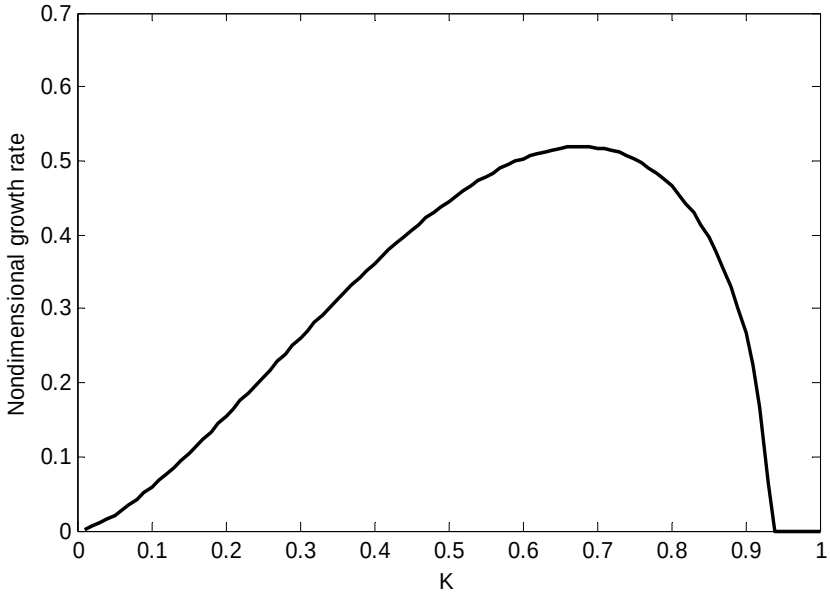

Figure 7. Nondimensional growth rate of an antisymmetrical disturbance without thermal modulation at $Q = 0.1$ and $We_2 = 1$.

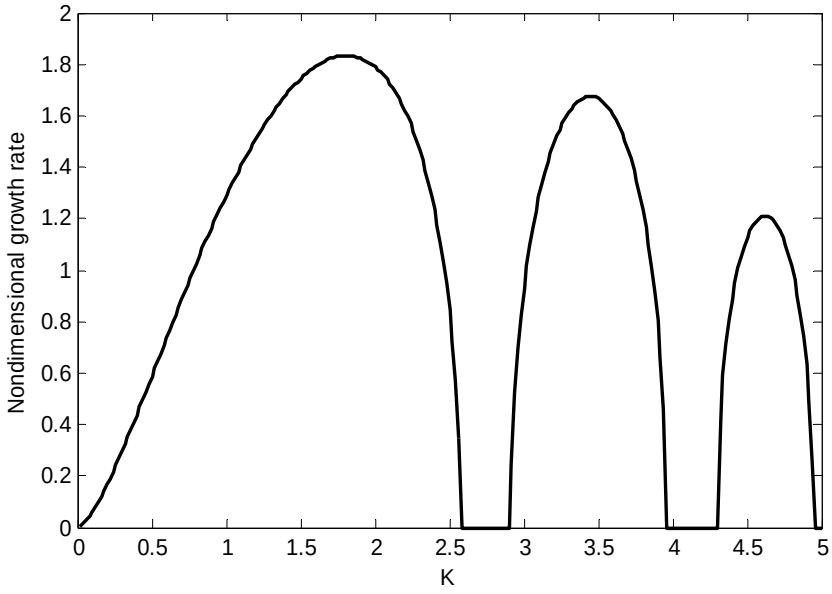

Figure 8. Nondimensional growth rate of a symmetrical disturbance with thermal modulation ($\hat{\omega} = 1$, $\varepsilon = 0.5$) at $Q = 0.1$ and $We_2 = 3$.

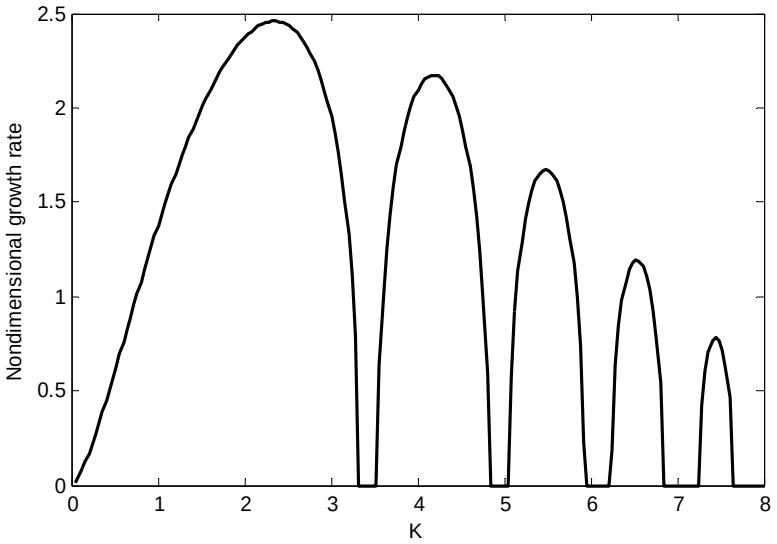

Figure 9. Nondimensional growth rate of a symmetrical disturbance without thermal modulation ($\hat{\omega} = 1$, $\varepsilon = 0.5$) at $Q = 0.1$ and $We_2 = 4$.

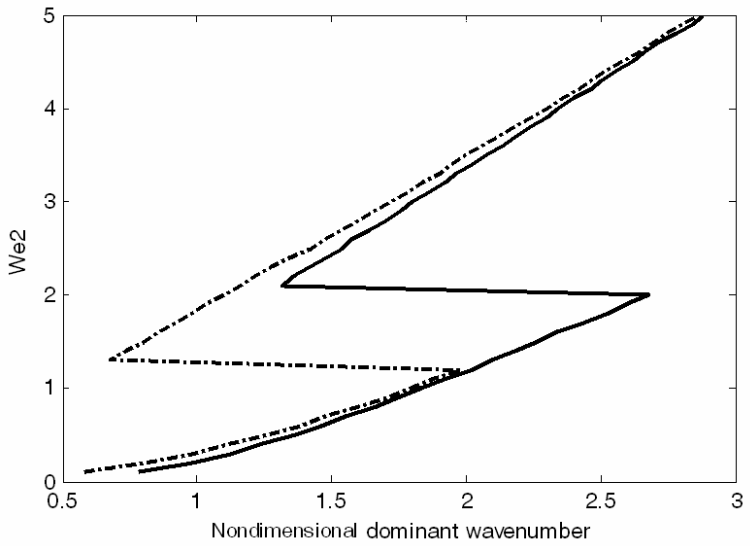

Figure 10. Nondimensional dominant wavenumber for an inviscid liquid sheet with thermal modulation ($\hat{\omega} = 1$, $\varepsilon = 0.5$). $Q = 0.1$. Solid curve: symmetrical disturbance; dash curve: antisymmetrical disturbance.

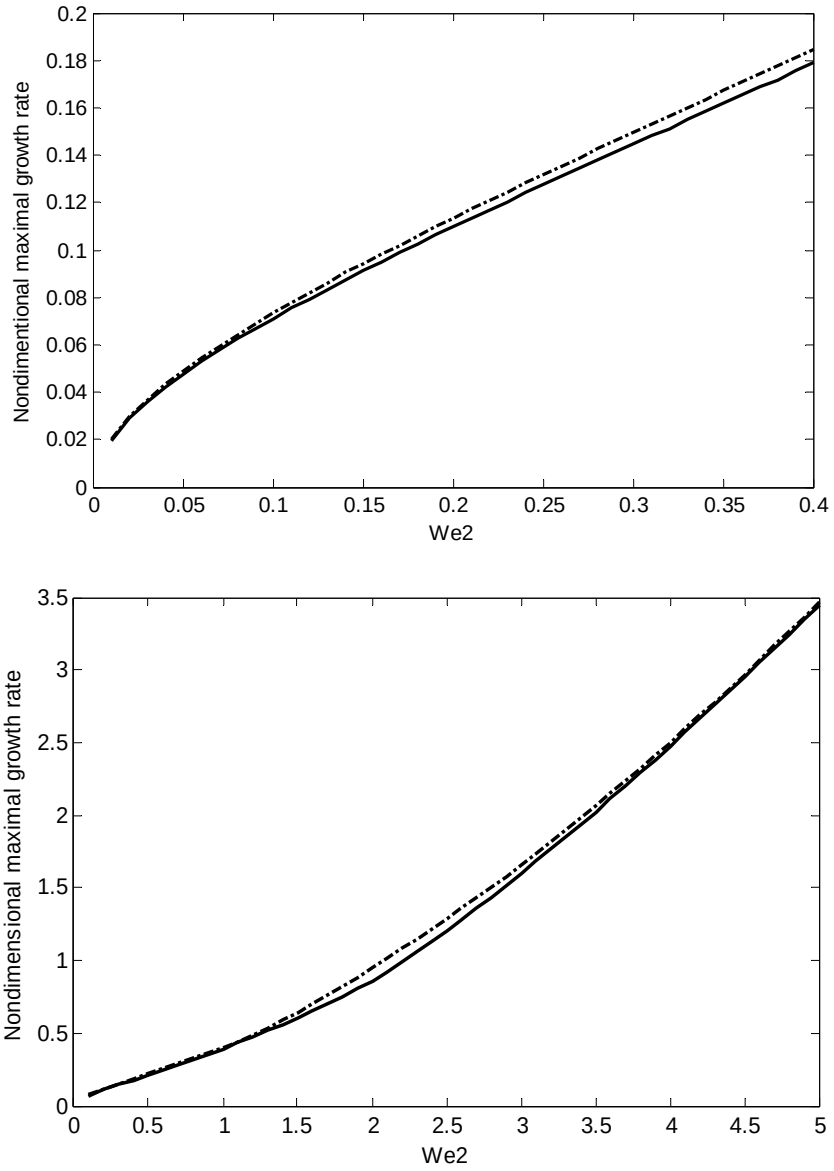

Figure 11. Nondimensional maximum growth rate for an inviscid liquid sheet with thermal modulation ($\hat{\omega} = 1$, $\varepsilon = 0.5$) at $Q = 0.1$. Solid curve: symmetrical disturbance; dash curve: antisymmetrical disturbance. In the top figure, detail at small gas Weber number is given.

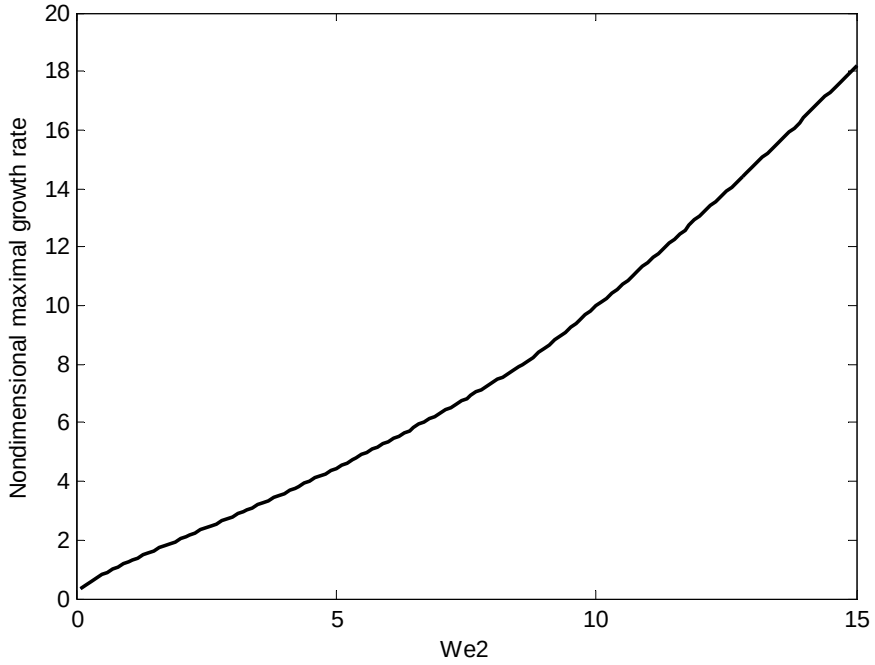

Figure 12. Nondimensional maximum growth rate for inviscid liquid sheet with thermal modulation ($\hat{\omega} = 5$, $\varepsilon = 0.5$) at $Q = 0.1$. Solid curve: symmetrical disturbance; dash curve: antisymmetrical disturbance.

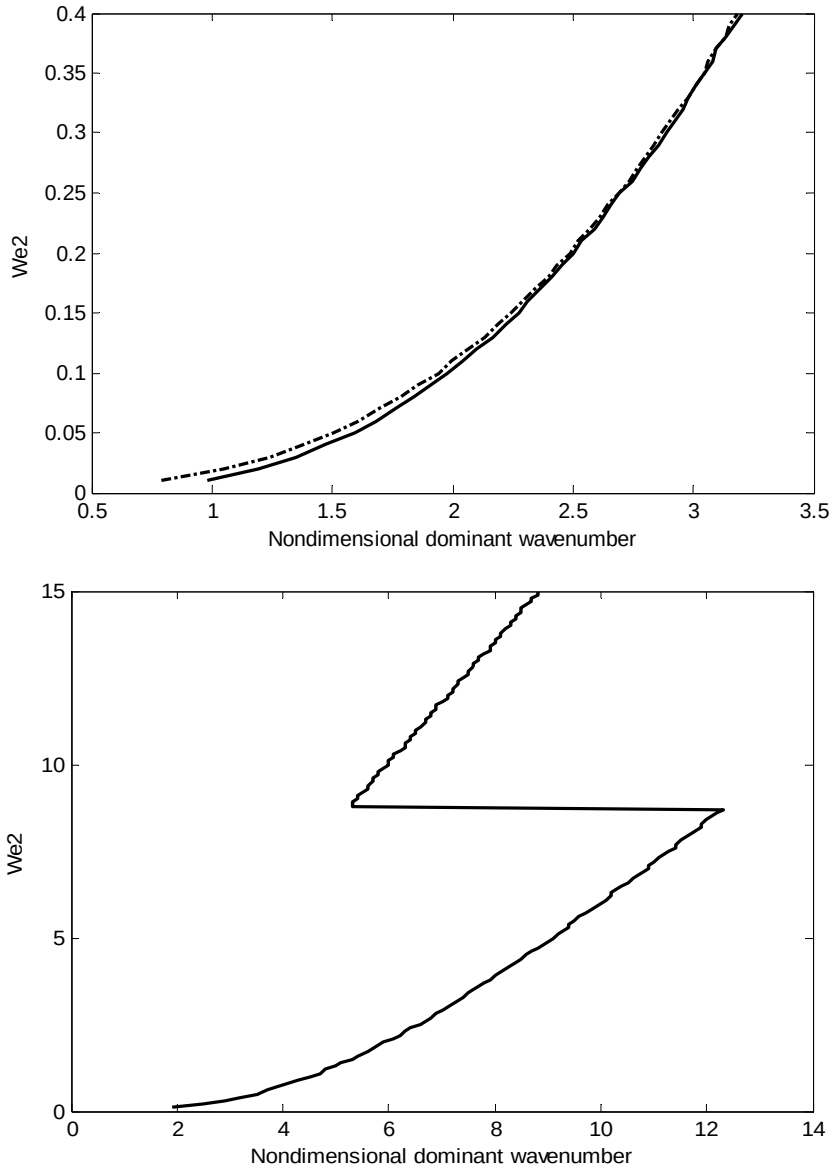

Figure 13. Nondimensional whole dominant wavenumber for inviscid liquid sheet with thermal modulation ($\hat{\omega} = 5$, $\varepsilon = 0.5$). $Q = 0.1$. Solid curve: symmetrical disturbance: dash curve: antisymmetrical disturbance.

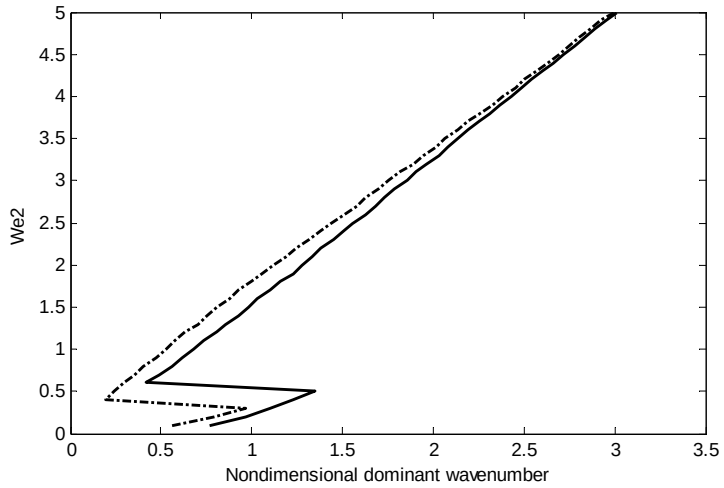

Figure 14. Nondimensional whole dominant wavenumber for inviscid liquid sheet with thermal modulation ($\hat{\omega} = 1$, $\varepsilon = 0.2$). $Q = 0.1$. Solid curve: symmetrical disturbance; dash curve: antisymmetrical disturbance.

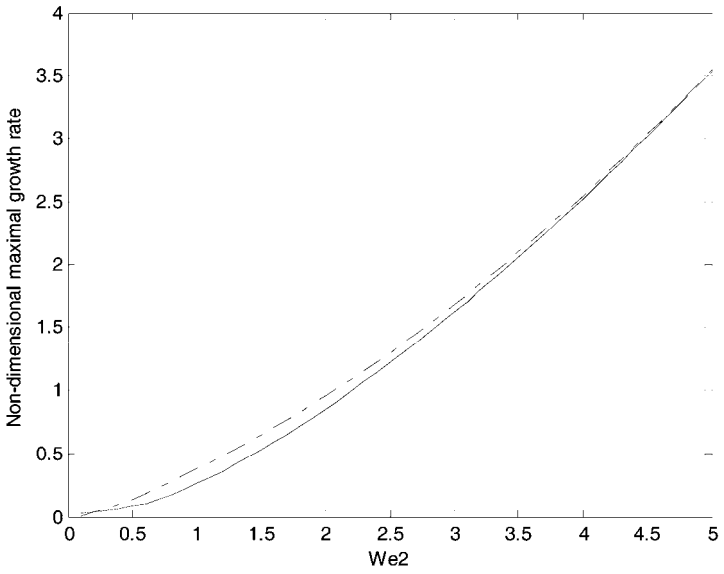

Figure 15. Non-dimensional maximum growth rate for inviscid liquid sheet with thermal modulation ($\hat{\omega} = 1$, $\varepsilon = 0.2$). $Q = 0.1$. Solid curve: symmetrical disturbance; dash curve: antisymmetrical disturbance.

References

[1] C. Clanet and E. Villermaux, Life of a smooth liquid sheet, J. Fluid Mech. 462 (2002), 307-340.

[2] N. Dombrowski and P. C. Hooper, The effect of ambient density on drop formation in sprays, Chem. Engng. Sci. 13 (1962), 291-305.

[3] W. W. Hagerty and J. F. Shea, A study of the stability of plane fluid sheets, J. Appl. Mech. 22 (1955), 509-514.

[4] I. Kim and W. A. Sirignano, Three-dimensional wave distortion and disintegration of thin planar sheets, J. Fluid Mech. 410 (2000), 147-183.

[5] X. Li and R. S. Tankin, On the temporal instability of a two-dimensional viscous liquid sheet, J. Fluid Mech. 226 (1991), 425-443.

[6] A. Mansour and N. Chigier, Dynamic behavior of liquid sheets, Phys. Fluids A 3 (1991), 2971-2980.

[7] P. Marmottant and E. Villermaux, On spray formation, J. Fluid Mech. 498 (2004), 73-111.

[8] J. Park, K. Kuh, X. Li and M. Renksizbulut, Experimental investigation on cellular breakup of a planar sheet from an air-blast nozzle, Phys. Fluids 16 (2004), 625-632.

[9] W. A. Sirignano and C. Mehring, Review of theory of distortion and disintegration of liquid streams, Progress in Energy and Combustion Science 26 (2000), 609-655.

[10] H. B. Squire, Investigation of instability of a moving liquid film, Br. J. Appl. Phys. 5 (1953), 167-169.